Monthly Notices
of the
ROYAL ASTRONOMICAL SOCIETY

MNRAS **466,** 3951–3960 (2017)
Advance Access publication 2016 December 20

doi:10.1093/mnras/stw3320

Spectral and time series analyses of the Seyfert 1 AGN: Zw 229.015

Oluwashina Adegoke,[1⋆] Suvendu Rakshit[2⋆] and Banibrata Mukhopadhyay[1⋆]

[1]*Astronomy and Astrophysics Programme, Department of Physics, Indian Institute of Science, Bangalore 560012, India*
[2]*Indian Institute of Astrophysics, Bangalore 560034, India*

Accepted 2016 December 16. Received 2016 December 14; in original form 2016 October 26

ABSTRACT

We analyse the spectra of the archival *XMM–Newton* data of the Seyfert 1 AGN Zw 229.015 in the energy range 0.3–10.0 keV. When fitted with a simple power law, the spectrum shows signatures of weak soft excess below 1.0 keV. We find that both thermal Comptonization and relativistically blurred reflection models provide the most acceptable spectral fits with plausible physical explanations to the origin of the soft excess than do multicolour disc blackbody and smeared wind absorption models. This motivated us to study the variability properties of the soft and the hard X-ray emissions from the source and the relationship between them to put further constraints on the above models. Our analysis reveals that the variation in the 3.0–10.0 keV band lags that in the 0.3–1.0 keV by 600^{+290}_{-280} s, while the lag between the 1.0-10.0 keV and 0.3–1.0 keV is 980^{+500}_{-500} s. This implies that the X-ray emissions are possibly emanating from different regions within the system. From these values, we estimate the X-ray emission region to be within $20R_{\rm g}$ of the central supermassive black hole (where $R_{\rm g} = GM/c^2$, M is the mass of black hole, G Newton's gravitational constant and c the speed of light). Furthermore, we use *XMM–Newton* and *Kepler* photometric light curves of the source to search for possible non-linear signature in the flux variability. We find evidence that the variability in the system may be dominated by stochasticity rather than deterministic chaos which has implications for the dynamics of the accretion system.

Key words: galaxies: active – galaxies: individual: Zw 229.015 – galaxies: Seyfert – X-rays: galaxies.

1 INTRODUCTION

The luminosity of an active galactic nucleus (AGN) originates from an accretion disc around the supermassive black hole usually in the optical/UV/EUV energy bands. A hard power law generally dominates above 2.0 keV and is believed to emanate from a hot corona or a sub-Keplerian flow (Bhattacharya, Ghosh & Mukhopadhyay 2010) made up of very high energy plasma ($\lesssim$ 150 keV) whose geometry is still not well understood. This means the optical/UV photons from the disc undergo inverse Compton scattering into X-ray energies and, as such, part of this energy in turn illuminates the disc and the other part is seen as the direct power law. The part that illuminates the disc is either subsequently reflected or thermalized (Mushotzky, Done & Pounds 1993). AGNs have been known to vary in their luminosities in all wavelengths and the study of the underlying mechanisms have proved to be efficient in helping us to understand the central region of AGNs.

Zw 229.015 is a Seyfert 1 AGN at a redshift $z = 0.028$ having a low galactic absorption column density ($N_{\rm H} \approx 6.25 \times 10^{20}{\rm cm}^{-2}$). Despite being relatively bright, its position in the galactic plane has resulted in there being very little known about this source (Carini & Ryle 2012). Its Seyfert nature was noted by Proust (1990) and it was observed in the *ROSAT* all sky survey by Zimmermann et al. (2001). Barth et al. (2011) carried out a ground-based reverberation mapping campaign on the source to complement its scheduled observation with the *Kepler* mission. They detected strong variability in the source exhibiting more than a factor of 2 change in its broad Hβ flux with Hβ full width at half-maximum (FWHM) of $2260 \pm 65\,{\rm km\,s}^{-1}$. By combining the measured Hβ lag with the broad Hβ width measured from the *rms* variability spectrum, they obtained a virial estimate of the mass of the supermassive black hole to be $\sim 10^7 {\rm M}_\odot$. More so, they obtained an estimate of its bolometric luminosity $L_{\rm bol} \sim 6.4 \times 10^{43}{\rm erg\,s}^{-1}$ and $L_{\rm bol}/L_{\rm Edd} \approx 0.05$. Edelson & Mushotzky (2011) reported a return of the source to its prior X-ray flux by 2011 July after an earlier report of a dramatic decrease in its flux variability in early June 2011 (Mushotzky & Edelson 2011). These observations reveal that the source is highly variable.

Edelson et al. (2014) utilized two methods of power spectral analysis to investigate its optical variability and search for the evidence of a bend frequency associated with a characteristic optical variability time-scale. They found it to be $\sim$5 d using the full *Kepler* data set of the source. It should be noted that Zw 229.015 exhibits strong and rapid variability in comparison with

⋆ E-mail : adegoke@physics.iisc.ernet.in (OA); suvendu.rakshit@iiap.res.in (SR); bm@physics.iisc.ernet.in (BM)

Table 1. Details of observation.

XMM–Newton	Parameters
Observation ID	0672530301
Start time for PN	2011-06-05 14:07:22
Stop time for PN	2011-06-05 21:35:10
Start time for MOS1	2011-06-05 13:39:02
Stop time for MOS1	2011-06-05 21:39:16
Start time for MOS2	2011-06-05 13:39:04
Stop time for MOS2	2011-06-05 21:39:16
EPIC filter	Medium
Mode(PN)	PrimeLargeWindow
Mode (MOS)	PartialPrimeW3

many other objects having a similar black hole mass and luminosity. It is also one of the few low-redshift Seyfert galaxies being monitored by *Kepler* with over three years of continuous observation. Hence, it is likely that Zw 229.015 will be a very important source for studying AGN properties. *Kepler* has been observing $\sim$115 deg^2 of the sky, monitoring $\sim$165 000 sources every 29.4 min with unprecedented stability ($\leq$0.1 per cent error for a 15th magnitude source) and high (>90 per cent) duty cycle over a period of several years (Mushotzky & Edelson 2011). With respect to timing and time series analysis, Bachev, Mukhopadhyay & Strigachev (2015) used the correlation integral (CI) method to search for signatures of chaos in the AGN W2R 1926+42 using its *Kepler* light curves. They reported the system to be stochastic. However, this time series method has not been applied to Zw 229.015.

In this paper, we report the result of the spectral analysis of Zw 229.015 using its *XMM–Newton* X-ray data which, to the best of our knowledge, has not been properly reported in the literatures prior to this time. We also report the result of our timing analyses of the source using its *XMM–Newton* and *Kepler* light curves. We assume a cosmology with $H_0 = 70\,\mathrm{km\,s^{-1}\,Mpc^{-1}}$, $\Omega_\mathrm{M} = 0.3$, $\Omega_\Lambda = 0.7$. Errors are quoted at the 90 per cent confidence level for one parameter of interest unless otherwise mentioned.

This paper is structured as follows. In Section 2, we describe the observation and data reduction procedure. Section 3 focuses on the spectral analysis, Section 4 reports the time series analyses from both the *XMM–Newton* X-ray data and *Kepler*'s optical data and Section 5 centres on discussions based on our analyses. Finally, in Section 6 we present a summary of our work.

2 OBSERVATIONS AND DATA REDUCTION

Zw 229.015 was observed on 2011 June 5 by *XMM–Newton* operated with medium filter. The observations with the EPIC-PN (Turner et al. 2001) and MOS (Strüder et al. 2001) detectors were of $\sim$27 ks and $\sim$29 ks durations, respectively, in all large window mode. We use the EPIC data for our analysis because it covers the energy range of interest to us (0.15–12.0 keV). Table 1 shows the details of the *XMM–Newton* observation. Although the addition of the MOS data to the spectral fit does not significantly improve the precision with which spectral parameters are determined, we decide to include it for completeness.

Data reduction for the *XMM–Newton* data follows standard procedure using the Science Analysis System software (SAS version 14.0.0) with updated Current Calibration Files (CCFs). Event files for the PN and MOS detectors are generated using the tasks EPPROC and EMPROC, respectively. These tasks allow for calibration of the energy and the astrometry of the events registered in each CCD chip and combines them into a single data file. Event file list is extracted using the SAS task EVSELECT. Data from the PN and MOS cameras are screened individually for time intervals with high background when the total count rate in the instrument exceeds 0.35 and 0.40 counts s^{-1} for the MOS and PN detectors, respectively. Good time interval (gti) files are generated after the intervals of the identified flaring particle background have been excluded based on the mentioned count rate cut off criteria. Cleaned event lists are subsequently obtained in line with the SAS standard procedure. Source photons are extracted from a circular region of radius 40 arcsec around the position of the source. Background is estimated from an annulus surrounding the source in each CCD. The X-ray spectra and light curves are generated using EVSELECT and background scaling factors are obtained using the task BACKSCALE. The ancillary and photon redistribution matrices are computed using the SAS tasks ARFGEN and RMFGEN, respectively. The resulting spectra are then grouped to have a minimum of 20 counts per bin to facilitate the use of the χ^2 minimization technique. Finally, the MOS1 and MOS2 spectra are added to generate a single spectrum with the ADDASCASPEC utility.

The *Kepler* data used in timing analysis are obtained during quarters 3–17 corresponding to the period between 2010 March and 2013 May. *Kepler's* long cadence and short cadence light curves have integration time of $\sim$30 min and $\sim$1 min, respectively. The *Kepler* pipeline (Jenkins et al. 2010) operates on original spacecraft data to produce calibrated pixel data (Quintana et al. 2010). The next step involves the extraction of the SAP-flux and finally the PDC-flux in which the light curves have been conditioned for transit searches. Therefore, we use the Simple Aperture Photometric (SAP) data in which long-term trends have not been removed from the light curves.

3 SPECTRAL ANALYSIS

Using XSPEC[1] (Arnaud 1996), we fit the *XMM–Newton* EPIC-PN and MOS spectra with a power-law distribution. We use the absorption model WABS (Morrison & McCammon 1983) to account for the galactic absorption of X-rays. We set the equivalent hydrogen column density N_H to $6.25 \times 10^{20}\,\mathrm{cm^{-2}}$ as obtained from the column density calculator (Kalberla et al. 2005). We keep this value fixed for all spectral analysis presented in this paper. During the fitting process, we introduce a normalization constant to account for the relative cross-calibration of the detectors. We carry out the fitting in the energy range 0.3–10.0 keV. Although the power law fits the spectra accurately well in the energy range 1.0–10.0 keV, when extrapolated to lower energies, we notice the presence of a weak soft excess, not uncommon though, it is especially weak for this source. We find the photon index to be 2.04 $\pm$ 0.06 and the $\chi^2/d.o.f.$ value to be 2050/1410. The spectra are shown in Fig. 1. Because the origin of the soft excess is still ill-understood, we set out to use four different physical models to fit the spectra and see which gives the best possible explanation for the origin of the soft excess. The results of fitting with the different models are given below.

3.1 Multicolour disc blackbody model

We fit the soft excess with a multicolour disc blackbody and a power law using the DISKBB model (Mitsuda et al. 1984;

[1] https://heasarc.gsfc.nasa.gov/xanadu/xspec/

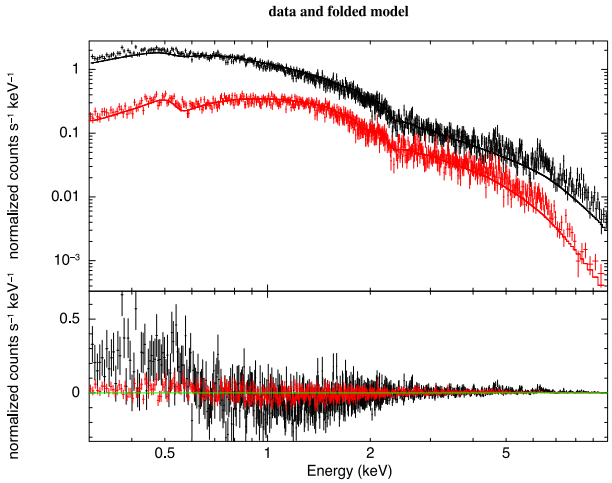

Figure 1. The combined EPIC-PN (black upper) and MOS (red lower) spectra of Zw 229.015 fitted with a power law. Signatures of some soft excess is seen below 1.0 keV as evident in the residue (lower) plot. [A colour version of this figure is available in the online version.]

Makishima et al. 1986). Here we consider the soft excess to result from an optically thick, geometrically thin Shakura–Sunyaev accretion disc (Shakura & Sunyaev 1973) around the AGN. The power-law photon index and the temperature of the inner disc are kept as free parameters. On fitting, the photon index obtained is 1.80 ± 0.01 implying a hard power law and the temperature of the inner disc is 156 ± 4 eV. This is, however, in agreement with literature (e.g. Gierliński & Done 2004; Bhattacharyya et al. 2014). The $\chi^2/d.o.f.$ value obtained is 1491/1408 which implies a reasonably good fit, but the inner disc temperature appears to be quite high and may be absurd for a Shakura–Sunyaev disc. This is represented in Fig. 2 (upper panel, left). Table 2 shows the detailed model parameters.

3.2 Smeared wind absorption model

This model considers an atomic origin for the soft excess emission. As explained by Gierliński & Done (2004), the soft excess could be a consequence of smeared absorption from partially ionized material (Dewangan et al. 2007). The explanation being that the soft excess is the result of smeared absorption from a partially ionized wind in an accretion disc. To assess this possibility, we fit the data

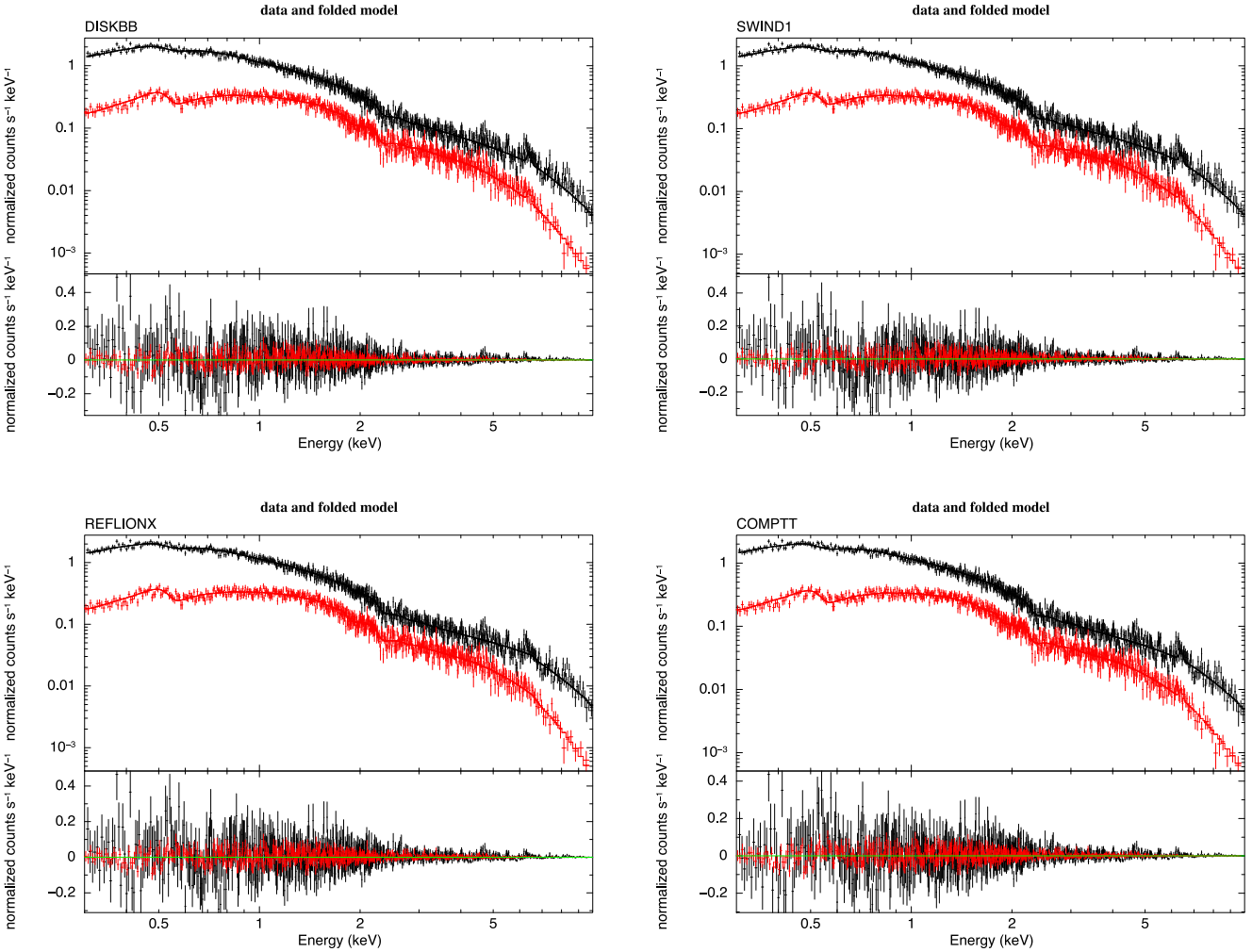

Figure 2. Upper panels: the combined EPIC PN (black upper) and MOS (red lower) spectra of Zw 229.015 fitted with a power-law *and* diskbb model (left); power-law *and* swind1 model (right). Lower panels: the combined EPIC PN (black upper) and MOS (red lower) spectra of Zw 229.015 fitted with a power-law *and* relativistically blurred reflection model (left); power-law *and* Comptonization model (right). [A colour version of this figure is available in the online version.]

Table 2. The best-fitting parameters and values from the spectra fitting of the *XMM–Newton* data of Zw 229.015.

Model/parameter and **best-fitting values**	
Model	constant*wabs*(diskbb+zpo)
Calibration factor (CF)	0.993 ± 0.008
$T_{\rm in}$(keV)	0.156 ± 0.004
Photon index Γ	1.80 ± 0.013
$\chi^2/d.o.f.$	1491/1408
Flux (erg cm^{-2} s^{-1})	6.66×10^{-12}
L (erg s^{-1})	1.14×10^{43}
Model	constant*wabs*(swind1*zpo)
Calibration factor (CF)	0.993 ± 0.008
Col. density ($\times 10^{22}$ cm^{-2})	13.80 ± 2.27
Log(ξ/erg cm s^{-1})	3.11 ± 0.07
σ(in units of v/c)	0.38 ± 0.04
Photon index Γ	1.96 ± 0.01
$\chi^2/d.o.f.$	1439/1406
Flux (erg cm^{-2} s^{-1})	6.72×10^{-12}
L (erg s^{-1})	1.15×10^{43}
Model	constant*wabs*kdblur(atable{reflionx.mod} +zpo)
Calibration factor (CF)	0.991 ± 0.008
kdblur index	4.22 ± 1.45
$R_{\rm in}(\frac{GM}{c^2})$	3.999 ± 0.491
Inclination(deg)	30
Photon index Γ	1.52 ± 0.082
Fe/Solar	0.469 ± 0.095
Reflionx Xi (erg cm s^{-1})	2308.32 ± 658.28
$\chi^2/d.o.f.$	1436/1404
Flux (erg cm^{-2} s^{-1})	6.68×10^{-12}
L (erg s^{-1})	1.15×10^{43}
Model	constant*wabs*(comptt+zpo) *disc approximation*
Calibration factor (CF)	0.993 ± 0.008
T_0(keV)	0.03
KT_e(keV)	0.632 ± 0.232
Optical depth τ_p	8.72 ± 1.63
Photon index Γ	1.52 ± 0.10
$\chi^2/d.o.f.$	1435/1407
Flux (erg cm^{-2} s^{-1})	6.83×10^{-12}
L (erg s^{-1})	1.18×10^{43}

with the smeared wind absorption model SWIND1 in XSPEC. The parameters of this model include absorption column density, ionization parameter $\xi = L/nr^2$ (L is the luminosity of the radiation, r is the radius of the disc and n is the number density of the absorbing wind) and the Gaussian velocity dispersion of the wind (σ) in units of v/c. The full list of model parameters and their values are given in Table 2 and Fig. 2 (upper panel, right) shows the fitted spectrum with the residue. This model provides a good fit to the data with $\chi^2/d.o.f. = 1439/1406$. However, the smearing velocity ($\sigma \sim 0.4c$) required to smoothen the absorption lines to produce the observed soft excess is unphysically large. Similar results have been obtained when the model is applied to some other sources (e.g. Dewangan et al. 2007; Bhattacharyya et al. 2014). Through self-consistent simulations, Schurch & Done (2007, 2008) and Schurch, Done & Proga (2009) deduced that it is difficult to generate such winds (with sufficient blurring to give the observed soft excess) from an accretion disc driven by radiation or thermal pressure. On the other hand, magnetohydrodynamic simulations show that matter dominated centrifugally driven jets with large opening angles can be self-consistently produced from the accretion disc (Hawley & Krolik 2006). However, as inferred by Bhattacharyya et al. (2014), due to the low densities of such jets ($\sim$500 cm^{-3}) sufficient absorption of radiation may not be possible.

3.3 Relativistically blurred reflection model

This model posits that the soft excess component results from X-ray ionized reflection. In the model, back-scattering and fluorescence of X-rays in the disc coupled with radiative recombination cause elements with low ionization potentials, such as C, O, N, to become highly ionized. The fluorescent lines are broadened and blurred due to the high velocities of matter and strong gravitational effects in the inner region of the disc, thus the soft excess is a series of similarly broadened emission lines that blend together to give a continuous emission feature. The model was developed by Ross & Fabian (2005). In XSPEC, the component is implemented as a tabular model REFLIONX and convolved with a LAOR (Laor 1991) to account for the blurring of the emission lines from the disc around a spinning black hole, since massive black holes in galactic nuclei are likely to be rapidly spinning (Volonteri et al. 2005; Crummy et al. 2006). This model assumes a lamp post geometry in which the compact corona located above the black hole illuminates the accretion disc resulting in radial-dependent irradiation. Thus, the emissivity associated with the reflection is parametrized as $\varepsilon(r) \propto r^{-q}$ where q is the emissivity index. Far away from the black hole, the irradiation decreases as r^{-3}, but the light bending effect is strong in the central region focusing some fraction of

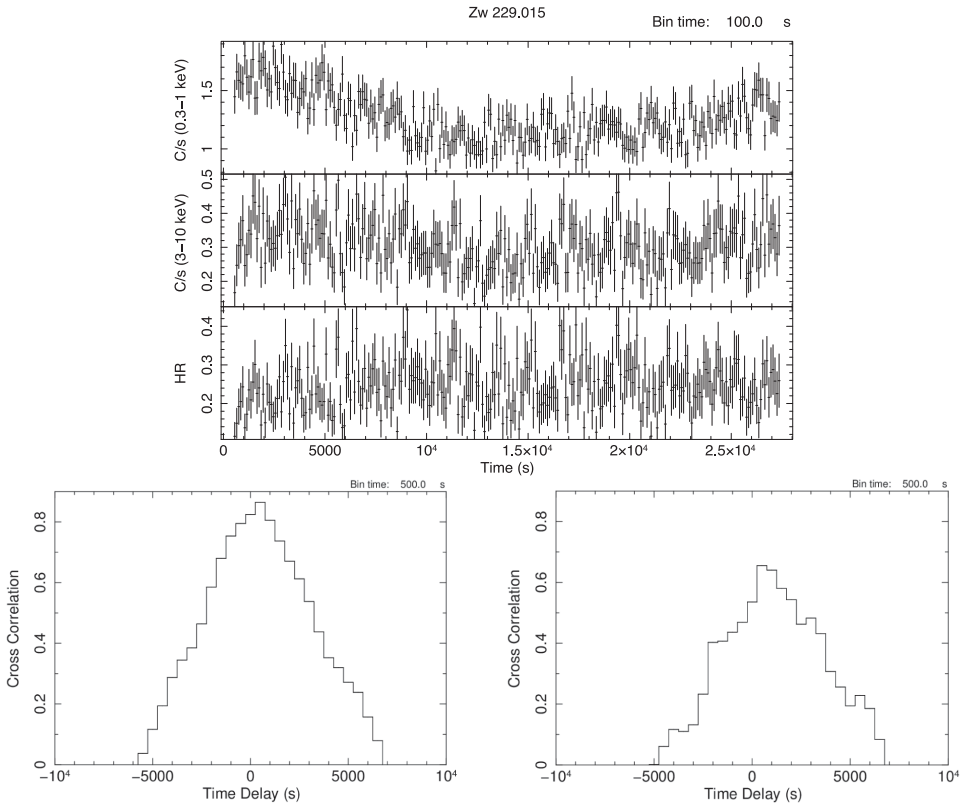

Figure 3. Upper panel: light curves of the energy bands 0.3–1.0 keV and 3.0–10.0 keV as well as the HR. Lower panels: CCF as a function of lag obtained using χ^2-minimization technique in XRONOS for the 0.3–1.0 keV *and* 3.0–10.0 keV variability (left) and 0.3–1.0 keV *and* 1.0–10.0 keV variability (right).

the coronal emission. Over the radial extent of the disc, the emissivity law can be approximated as a broken power law (Fabian et al. 2012).

The parameters of the model are emissivity index of the disc, ionization parameter, inclination of the disc, iron abundance of the accreting matter (elements higher than iron are considered to have solar abundance), spectral index of the power-law radiation, inner and outer radii of the disc. For the inclination, we fix a modest value of 30° since Seyfert 1 galaxies generally have low inclination angles. The outer radius is fixed at $400R_g$ ($R_g = GM/c^2$, where G is Newton's gravitational constant, M is the black hole mass and c is the speed of light) while the inner radius is kept free. All model parameters and their values are shown in Table 2. The $\chi^2/d.o.f.$ comes out to be 1436/1404. Fig. 2 (lower panel, left) shows the fitted spectrum and the residual.

3.4 Thermal Comptonization model

This model was developed by Titarchuk (1994). It is an analytic model that describes the Comptonization of soft photons in a hot plasma. The model assumes that seed photons emanating from the accretion disc are Compton-boosted by plasma in an optically thick medium, i.e. the thermal disc supplies energy for the Compton tail. The model includes relativistic effects and the approximations used work well for both optically thin and thick regimes. In this model, the so-called β-parameter (which has no dependence on geometry) and the plasma temperature fully describe the Comptonized spectrum. Subsequently, the optical depth is determined for a given geometry as a function of β. Parameters of the model include the photon index of the power-law component, the temperature of the seed photons, the optical depth and temperature of the Comptonizing plasma. The complete list of parameters and their fit values are provided in Table 2. The model is implemented as COMPTT in XSPEC. We fix the seed photon temperature to 30 eV since this is about the typical temperature for the inner region of a Shakura–Sunyaev accretion disc around a black hole of mass $10^7 M_\odot$. After fitting, the $\chi^2/d.o.f.$ value comes out to be 1435/1407. The model spectrum is shown in Fig. 2 (lower panel, right).

4 TIMING ANALYSIS

We extract light curves in the soft energy band 0.3–1.0 keV and hard bands 1.0–10.0 keV and 3.0–10.0 keV. This is based on the shape of the spectrum with bin times of 100 and 500 s in order to study the correlation between the soft and hard energy bands. Fig. 3 (upper panel) shows the light curves of the source in two of the mentioned energy bands as well as the light curve from the hardness ratio (HR) defined as the ratio of the flux in the 3.0–10.0 keV to that in the 0.3–1.0 keV in this case. The 0.3–1.0 keV band shows a trough-to-peak variation by a factor of ∼2.4, while the 3.0–10.0 keV band shows a trough-to-peak variation by a factor of ∼3.6, further corroborating the fact that the X-ray emissions from Zw 229.015 are highly variable. To investigate the possibility of a lag between the light curves of the soft (0.3–1.0 keV) and the hard (1.0–10.0 keV *and* 3.0–10.0 keV) energy bands, we carry out cross-correlation analysis on the light curves. Afterwards, to search for signatures of low-dimensional chaos (important for studying the disc dynamics) in the optical as well as X-ray variability of

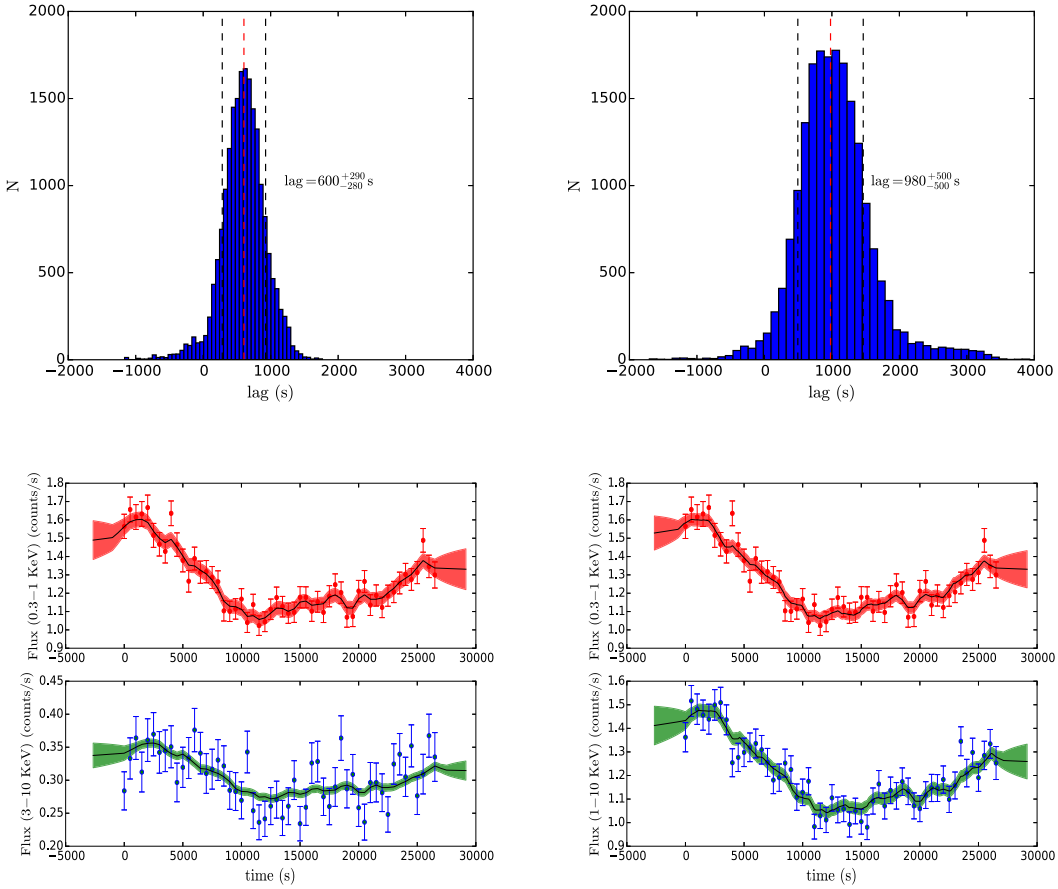

Figure 4. Upper panels: histogram showing the probability distribution of JAVELIN lag between the 0.3–1.0 keV *and* 3.0–10.0 keV (left) and 0.3–1.0 keV *and* 1.0–10.0 keV (right) X-ray variabilities. Lower panels: respective light curves of different bands obtained using the JAVELIN code. [A colour version of this figure is available in the online version.]

the source, we carry out non-linear timing analysis (Grassberger & Procaccia 1983) on the source.

4.1 Cross-correlation analysis

We use the XRONOS[2] Blackburn (1995) program *crosscor* to compute the cross-correlation function (CCF) between the soft and hard band light curves with 500 s bins. The variations of CCFs as functions of time delay between the soft and hard energy bands are shown in Fig. 3 (lower panels). In the CCF, visual inspection shows that the most prominent peaks in both the curves are at a positive time lag, implying that the hard band lags the soft (see e.g. Hernández-García et al. 2015). A time lag between the variability of the soft and hard X-ray bands has been reported for some AGNs before now (e.g. Gallo et al. 2004; Dasgupta & Rao 2006; Pal et al. 2016b) implying plausibly different emission regions for the soft excess and the hard power law for Seyfert 1 AGNs.

As mentioned by Dewangan et al. (2007), due to the complex nature of the shape of the CCF, the non-Gaussian distribution of the errors and the inter-dependence of the CCF data points, it is somewhat difficult to measure the statistical significance of the time lag from model fitting to the CCF using the χ^2 minimization technique. As a result, to estimate the lag and its uncertainty between soft and hard bands, we use the JAVELIN[3] code which is a PYTHON implementation of the SPEAR (Stochastic Process Estimation for AGN Reverberation; Zu, Kochanek & Peterson 2011). JAVELIN has been successful in predicting reliably time lags in AGN optical light curves. It uses a damped random walk (DRW; Kelly, Bechtold & Siemiginowska 2009; Zu et al. 2013) process to model the continuum emission in an AGN and then model the emission line light curve which is a smoothed, scaled and shifted version of the former. It estimates the best-fitting lag by comparing model light curves with the observed ones. After fitting this code to the data, we obtain a positive time lag of 600^{+290}_{-280} s between the 0.3–1.0 keV and 3.0–10.0 keV flux variability and 980^{+500}_{-500} s between the 0.3–1.0 keV and 1.0–10.0 keV flux variability, which implies that the hard X-ray lags the soft in its variability by an amount of this order. Significantly low signal-to-noise ratio (SNR) does not allow us to explore softer and harder bands. The plots of probability distribution functions of the lags as obtained from JAVELIN fit are shown by the histogram in Fig. 4 (upper panels), while the lower panels show the best-fitting light curves of different bands as obtained from the code. The relatively large uncertainties are possibly due to the data quality. Worthy of note is the fact that the results obtained through *crosscor* and the JAVELIN code are in good agreement. This leads us to the conclusion that the lag will not be more than ∼1000 s. This observed time lag definitely puts a

[2] http://heasarc.gsfc.nasa.gov/docs/xanadu/xronos/xronos.html

[3] http://www.astronomy.ohio-state.edu/yingzu/codes.html

further constraint on the tenable model to explain the origin of the soft excess.

4.2 Non-linear timing analysis

We apply the non-linear time series analysis technique to search for signatures of low-dimensional chaos in the X-ray and optical light curves of Zw 229.015 using its *XMM–Newton* and *Kepler* data, respectively. We use the CI method.

One of the standard methods for reconstructing the dynamics of a non-linear system from a time series is the delay embedding technique (Grassberger & Procaccia 1983). The idea is to construct a CI equal to the probability that two arbitrary points in phase space are closer together than some separation R. Since the dimension of the system (i.e. the number of governing equations or variables) is not a priori known, one has to construct the dynamics for different embedding dimensions M. In this technique, vectors of dimension M are created from the time series $s(t_i)$ using a delay time τ such that

$$\boldsymbol{x}(t_i) = [s(t_i), s(t_i + \tau), s(t_i + 2\tau), ..., s(t_i + (M-1)\tau)]. \quad (1)$$

Typically, τ is suitably chosen such that the vectors are not correlated, i.e. when the autocorrelation function of $\boldsymbol{X}(t_i)$ approaches zero or when it attains its first minima.

Correlation dimension: this provides a quantitative picture of the reconstructed dynamics. The computational procedure involves choosing a large number of points in the reconstructed dynamics as centres. The CI $C_M(R)$ is the number of points that are within the distance R from the centre averaged over all the centres and is written as

$$C_M(R) = \frac{1}{N(N_c - 1)} \sum_{i=1}^{N} \sum_{j \neq i}^{N_c} \sum_{j=1} H(R - |\boldsymbol{x}_i - \boldsymbol{x}_j|), \quad (2)$$

where $\boldsymbol{x}_i, \boldsymbol{x}_j$ are the reconstructed vectors, H is the Heaviside step function, N is the number of points and N_c the number of centres. The correlation dimension D_2 is essentially the scaling index of the variation of $C_M(R)$ with R and it is expressed as

$$D_2 = \lim_{R \to 0} \left(\frac{d\log C_M(R)}{d\log R} \right). \quad (3)$$

Knowledge of D_2 allows one to determine the effective number of differential equations describing the dynamics of the system in principle. More details on this technique and its interpretation can be found in the works of Misra et al. (2006) and Bachev et al. (2015) to mention but a few. D_2 can be calculated from the linear part of the plot of $\log[C_M(R)]$ against $\log[R]$ and its value depends on the value of M. The plot of D_2 against M can reveal the non-linear dynamical properties of the system. If $D_2 \approx M$ for all M, then the system is stochastic; however for a deterministic system, initially D_2 increases linearly with M until it reaches a certain value and saturates. This saturated value of D_2 is taken to be the correlation/fractal dimension of the system. Worthy of mention is the fact that a saturated D_2 is a necessary but not a sufficient condition for chaos. The existence of colour noise in a stochastic system may lead to a saturated D_2 of low value as well. Therefore, it is customary to analyse the data by an alternative approach to distinguish it from a pure noisy time series. To do this, one applies the surrogate data analysis technique (Theiler et al. 1992). Simply put, surrogate data are random data generated by taking the original signal and reprocessing it so that it has the same distribution and power spectrum as the original data but has lost all its deterministic characteristics (i.e. phase randomization).

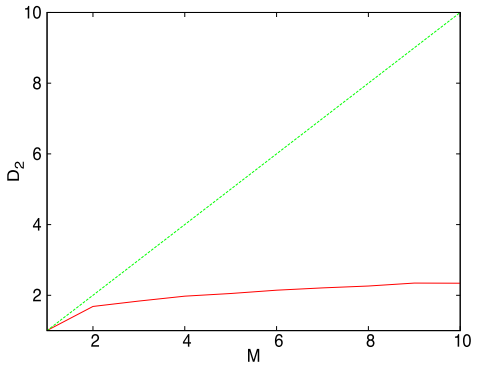

Figure 5. The variation of correlation dimension as a function of embedding dimension for the Lorenz system showing saturation at low D_2 (red solid line). The green dashed line along the diagonal of the figure indicates an ideal stochastic curve. [A colour version of this figure is available in the online version.]

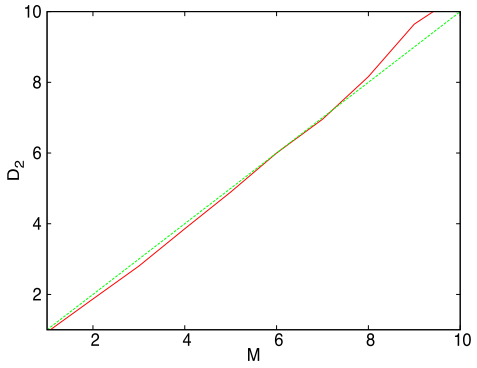

Figure 6. The variation of correlation dimension as a function of embedding dimension from *XMM–Newton* EPIC-PN data showing the stochastic nature of its X-ray light curve (red solid line). The green dashed line shows the behaviour of an ideal stochastic system. [A colour version of this figure is available in the online version.]

Then the same analysis is carried out on the surrogates to identify any distinguishing features. The scheme proposed by Schreiber & Schmitz (1996) known as the Iterative Amplitude Adjusted Fourier Transform (IAAFT) is more consistent to generate surrogates.

Before applying the CI method to real data, we apply it to the light curve from the Lorenz system which is known to exhibit fractal dimension ($D_2 = 2.06$) for a particular parameter $R = 28$ [not the same as R used in the $C_M(R)$ equation]. Fig. 5 confirms that the Lorenz system is indeed chaotic, showing the variation of correlation dimension as a function of embedding dimension. On applying the CI method to the *XMM–Newton* and the *Kepler* data, no saturation is observed in the variation of D_2 with M as shown in Figs 6 and 7, respectively. While the *Kepler* data exhibit D_2 deviating from the ideal stochastic curve, D_2 for *XMM–Newton* data practically overlap with that of stochasticity. We do not consider including surrogate data here since the original light curves do not show signatures of chaos. More so, the $D_2 - M$ curves for surrogates and the original data from the *Kepler* light-curve overlap (not shown in Fig. 7). Based on this analysis, we infer that the X-ray and optical light curves of Zw 229.015 are dominated plausibly by stochastic noise rather than deterministic chaos. The implication of this could be that advection is an important component of the accretion flow dynamics with random cooling processes (general advective accretion flow; Rajesh &

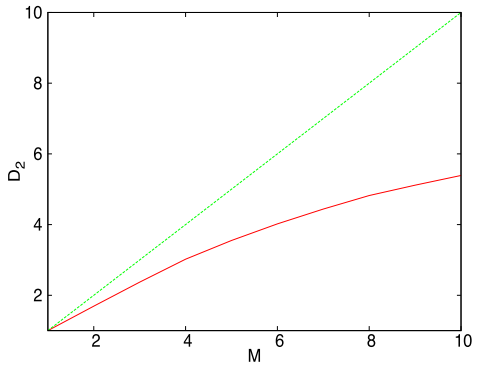

Figure 7. The variation of correlation dimension as a function of embedding dimension from the *Kepler* short cadence data; it reveals the stochastic nature of the optical light curve of the system (red solid line). The green dashed line shows the behaviour of an ideal stochastic system. [A colour version of this figure is available in the online version.]

Mukhopadhyay 2010) destroying any signature of self-similarity in the flux variability, making it stochastic.

5 DISCUSSIONS

We have analysed the archival *XMM–Newton* and *Kepler* photometric data for Zw 229.015 with the aim of understanding the spectral and timing behaviours of the source and to search for possible correlation between them. The X-ray energy range considered here is 0.3–10.0 keV, which is fairly well fitted with a simple power law except for the presence of some soft excess noticed below 1.0 keV.

5.1 The soft excess

In order to understand the origin of the soft excess, motivated by the work of Dewangan et al. (2007), Bhattacharyya et al. (2014) and several others, we apply four models in fitting the EPIC-PN and MOS spectra of the source. The models are multicolour disc blackbody model, smeared wind absorption model, relativistically blurred reflection model and thermal Comptonization model. Worthy of mention is the fact that the smeared wind absorption model and the relativistically blurred reflection model relate the soft excess to atomic processes in the disc.

The disc temperature that we have obtained from the DISKBB fit is 156 eV which is much higher than the predicted value for an optically thick, geometrically thin accretion disc around a black hole of mass $\sim 10^7\,\mathrm{M}_\odot$. From standard accretion disc theory (Novikov & Thorne 1973; Shakura & Sunyaev 1973), the approximate temperature of the disc blackbody at a radius r is given by

$$T_{\rm eff}(r) \sim 6.3 \times 10^5 \left(\frac{\dot{M}}{\dot{M}_{\rm Edd}}\right)^{1/4} \left(\frac{M}{10^8 \mathrm{M}_\odot}\right)^{-1/4} \left(\frac{r}{r_{\rm s}}\right)^{-3/4} \mathrm{K}, \quad (4)$$

where $\dot{M}$ is the black hole accretion rate, $\dot{M}_{\rm Edd}$ is the Eddington accretion rate, $\dot{M}/\dot{M}_{\rm Edd}$ is the scaled accretion rate and $r_{\rm s}$ is the Schwarzschild radius of the black hole given as $r_{\rm s} = 2R_{\rm g}$. Thus for a non-spinning black hole of this mass, taking $r = 3r_{\rm s}$, the value of the disc temperature will be $\sim$30 eV. Done et al. (2012) proposed the idea of colour temperature correction to AGN disc spectrum but eventually they came up with the conclusion that even though the colour temperature correction is substantial, it is not sufficient to account for the origin of the soft excess. Furthermore, the temperature of this component is fairly constant and not related to the luminosity and mass of the black hole (Gierliński & Done 2004). However, the disc model predicts that the disc temperature should be correlated with the black hole mass. Thus, the possibility of Compton scattering of photons could be important. Within the observed energy band, the spectrum does not show any cut-off which implies that it is not possible to constrain the temperature of the corona, as such observing the source in hard X-rays may help to ascertain the thermal Compton origin of the power law.

The smeared wind absorption model of Gierliński & Done (2004) posits that the soft excess emission is predominantly a consequence of strong and smeared absorption near $\sim$0.7 keV. The idea is that the soft excess and the hard power law are from the same continuum component but for the small contributions from smeared emission lines. This means, the soft and hard band emissions are from the same continuum component or physical process – Comptonization (Dewangan et al. 2007). However, there is a major problem with this absorption model which is that the predicted smearing velocity for the source ($\sim 0.4c$) is unphysically large for disc winds. As shown by hydrodynamic simulations, the line-driven winds do not have the required smearing velocity (e.g. Schurch et al. 2009). It remains to be confirmed if magnetically driven winds can provide the required smearing (Dewangan et al. 2007). Outflowing winds having velocities as high as $0.1 - 0.2c$ have been observed in a few sources with high accretion rates (e.g. Pounds et al. 2003), however, when we fix the smearing velocity to $0.1c$, we get unacceptably poor fits.

In the reflionx model, we have considered the soft excess as having an atomic origin in which case a hot corona produces the power-law continuum by the Comptonization of soft photons from the disc. These hard power-law photons irradiate the disc producing fluorescent secondary emissions which are subsequently blurred by the strong gravity in the vicinity of the black hole and the high velocities of the accreting material. In the reflection model, substantial fraction of the soft X-ray excess emission is due to the blurred reflection from the partially ionized material owing to lines and bremsstrahlung from the hot surface layers (Ross & Fabian 2005). According to Crummy et al. (2006), this model is best explained in the scenario of a small power-law illuminating region above the central black hole where light bending effects deflect the illuminating power-law radiation on to the disc and thus is not fully detected. Although there is no evidence for strong Fe Kα line in this source, such a line may be hidden in the strong X-ray continuum, which involves the reprocessing of the primary X-ray emission from the corona. This model naturally explains the constancy of the observed temperature seen in many sources which is a measure of atomic transition in this case as mentioned by D'Ammando et al. (2008).

In the thermal Comptonization model, we have modelled the soft excess in the energy range 0.3–1.0 keV by considering disc photon Comptonization in an optically thick thermal corona. The seed photon temperature is fixed at 30 eV (typical for a black hole mass $\sim 10^7 \mathrm{M}_\odot$). Corona temperature of $\sim$632 eV and $\sim$635 eV is obtained for disc and spherical geometries, respectively, while the optical depth comes out to be 8.7 and 18.1 for disc and spherical geometries, respectively. As noted by Noda (2016), the soft X-ray excess can be considered to be an additional primary emission rather than a contamination from a host galaxy or a secondary emission component. From the values of optical depths and plasma temperature that we obtain from this model, we conclude that the soft excess is likely to be produced in a relatively cool and dense corona which is clearly different from those producing the dominant power law in which case the plasma temperature is of the order of $\sim$150 keV and optical depth $<$1.0. The positive lag we have

obtained in the CCF analysis is in tandem with the prediction of the Comptonization model which is that the hard X-ray variation should lag the soft. The time lag in this case represents the difference in the photon escape times between the soft and the hard bands. This implies that the hard band photons tend to have undergone more scattering events and so travel longer and escape the corona later than the soft photons. Although, as reported by Gierliński & Done (2004) and Crummy et al. (2006), one caveat of this model is the relative constancy of the disc temperature (around 0.1–0.2 keV), regardless of the central object's luminosity and mass. More samples of AGNs have to be studied to shed more light on this and from our result, Comptonization from a cold corona is plausibly a major contributor to the soft excess emission.

5.2 Timing analysis

We have shown that the variability in the hard X-ray band lags the variability in the soft on a time-scale of ∼1000 s. This is interesting because on the one hand it reveals that they are most likely emitted from different regions of the accretion disc, a result that is consistent with the two corona model which posits that the soft X-ray photons may be the seed for the observed inverse Comptonized hard photons. Based on this lag, we estimate the size of the corona system around the black hole as

$$d = c \times t_{\rm lag}, \tag{5}$$

where d is the separation between the two coronae (i.e. the approximate extent of the coronae geometry) and $t_{\rm lag}$ is the measured lag. This gives a value of $d \sim 3 \times 10^{13}{\rm cm} = 20R_{\rm g}$. This indicates that the coronae system is very compact. Thus it is not surprising that the X-ray luminosity of the source is only $\sim 10^{43}{\rm erg\,s^{-1}}$ while beyond $20R_{\rm g}$, the disc is dominated by optical/UV emission. Although lags in the opposite sense have been reported on short time-scales in some AGNs (e.g. de Marco et al. 2011; Emmanoulopoulos, McHardy & Papadakis 2011; Tripathi et al. 2011; Zoghbi & Fabian 2011; Fabian et al. 2012; De Marco et al. 2013), this is not evident in our analysis.

We have shown that Zw 229.015 exhibits stochastic variability as seen from both its X-ray and optical light curves. The stochastic nature of the X-ray variability may be explained possibly by invoking the light bending effects. This has a strong influence on the brightness of the primary power-law source (and by extension, the reflected component), making it appear faint to a distant observer when it is close to the black hole and bright when further away. In this case we consider the variability of the emitted X-ray photons as plausibly intrinsic to the corona or due to the position of the corona relative to the hole (which may be a stochastic rather than a deterministic effect). The optical emission on the other hand is known to be produced from the optically thick, geometrically thin accretion disc and, according to Bachev et al. (2015), one way to account for the apparently stochastic optical light curve is to invoke a large number of active zones or emitting blobs. This implies that the overall light curve will be stochastic in nature irrespective of the exact injection mechanism in each zone. This is based on the assumption that deterministic injection will lead to deterministic optical variability, evidence for which we do not find. Moreover, the presence of significant advection component with random cooling within the flow is possible and this is to an extent corroborated by the value of $L_{\rm bol}/L_{\rm Edd}$ obtained for this source. The presence of such a component may result in random flux fluctuations and thus revealing the stochasticity seen in the X-ray light curve. It suffices to add that it is not surprising that both the X-ray and the optical variabilities of the source are stochastic since there is growing evidence that the X-ray and optical variations of Seyfert galaxies are correlated in some way (Arévalo et al. 2008; Breedt et al. 2009; Pal et al. 2016a).

6 SUMMARY

Based on the result of our spectral and timing analyses of Zw 229.015, we have come up with the following conclusions.

(i) The spectral analysis of the *XMM–Newton* X-ray data of the source in the energy range 0.3–10.0 keV reveals the presence of some soft excess emission below 1.0 keV and a power-law dominance above 1.0 keV.

(ii) Of the four models with which we have fitted the spectra, namely multicolour disc blackbody, smeared wind absorption, relativistically blurred reflection and the thermal Comptonization models, the thermal Comptonization and relativistically blurred reflection models give the most acceptable spectral fits and moreover they offer more physical explanation to the origin of the soft excess emission.

(iii) From the observation of a positive time lag of ∼1000 s between the soft and hard bands, we have inferred that the two are produced from different regions extending only up to $\sim 20R_{\rm g}$ which gives credence to the possibility of a thermal comptonization. We believe that future high-sensitivity broad-band measurements will hopefully give better constraints for Seyfert 1 AGNs.

(iv) From the non-linear time series analysis of the source, in both the X-ray and optical bands, we do not find signatures of low-dimensional chaos, thus buttressing the fact that X-ray and optical variabilities of Seyfert galaxies may be correlated in some way. Worthy of mention is the fact that although the CI method can provide an indication of non-linearity, it may also fail to detect non-linear behaviour. The test for the signature of non-linearity should be done by other methods as well in order to have a more conclusive statement. For example, the non-linear prediction error (Schreiber & Schmitz 1997) could be explored towards this mission, which we might indeed consider for future work. More so, because of the stochastic nature of the light-curve variability of the source, we conclude that the source may exhibit a non-standard accretion flow (having plausibly a significant advection component) as evident also from its low bolometric luminosity ($\sim 0.05L_{\rm Edd}$; Barth et al. 2011). This is already observed in many black hole systems. These features may, however, change with time as the source is known to be rapidly variable.

ACKNOWLEDGEMENTS

We acknowledge the anonymous referee for comments that improved this manuscript. We wish to thank Ramesh Narayan, Gulab Dewangan and C. S. Stalin for their valuable comments over the manuscript and suggestions. A partial financial support from the project with research Grant No. ISTC/PPH/BMP/0362 is also acknowledged.

REFERENCES

Arévalo P., Uttley P., Kaspi S., Breedt E., Lira P., McHardy I. M., 2008, MNRAS, 389, 1479

Arnaud K. A., 1996, in Jacoby G. H., Barnes J., eds, ASP Conf. Ser. Vol. 101, Astronomical Data Analysis Software and Systems V. Astron. Soc. pac., San Francisco, p. 17

Bachev R., Mukhopadhyay B., Strigachev A., 2015, A&A, 576, A17

Barth A. J. et al., 2011, ApJ, 732, 121
Bhattacharya D., Ghosh S., Mukhopadhyay B., 2010, ApJ, 713, 105
Bhattacharyya S., Bhatt H., Bhatt N., Singh K. K., 2014, MNRAS, 440, 106
Blackburn J. K., 1995, in Shaw R. A., Payne H. E., Hayes J. J. E., eds, ASP Conf. Ser. Vol. 77, Astronomical Data Analysis Software and Systems IV. Astron. Soc. Pac., San Francisco, p. 367
Breedt E. et al., 2009, MNRAS, 394, 427
Carini M. T., Ryle W. T., 2012, ApJ, 749, 70
Crummy J., Fabian A. C., Gallo L., Ross R. R., 2006, MNRAS, 365, 1067
D'Ammando F., Bianchi S., Jiménez-Bailón E., Matt G., 2008, A&A, 482, 499
Dasgupta S., Rao A. R., 2006, ApJ, 651, L13
de Marco B., Ponti G., Uttley P., Cappi M., Dadina M., Fabian A. C., Miniutti G., 2011, MNRAS, 417, L98
De Marco B., Ponti G., Cappi M., Dadina M., Uttley P., Cackett E. M., Fabian A. C., Miniutti G., 2013, MNRAS, 431, 2441
Dewangan G. C., Griffiths R. E., Dasgupta S., Rao A. R., 2007, ApJ, 671, 1284
Done C., Davis S. W., Jin C., Blaes O., Ward M., 2012, MNRAS, 420, 1848
Edelson R., Mushotzky R., 2011, The Astron. Telegram, 3484
Edelson R., Vaughan S., Malkan M., Kelly B. C., Smith K. L., Boyd P. T., Mushotzky R., 2014, ApJ, 795, 2
Emmanoulopoulos D., McHardy I. M., Papadakis I. E., 2011, MNRAS, 416, L94
Fabian A. C. et al., 2012, MNRAS, 419, 116
Gallo L. C., Boller T., Tanaka Y., Fabian A. C., Brandt W. N., Welsh W. F., Anabuki N., Haba Y., 2004, MNRAS, 347, 269
Gierliński M., Done C., 2004, MNRAS, 349, L7
Grassberger P., Procaccia I., 1983, Phys. Rev. A, 28, 2591
Hawley J. F., Krolik J. H., 2006, ApJ, 641, 103
Hernández-García L., Vaughan S., Roberts T. P., Middleton M., 2015, MNRAS, 453, 2877
Jenkins J. M. et al., 2010, ApJ, 713, L87
Kalberla P. M. W., Burton W. B., Hartmann D., Arnal E. M., Bajaja E., Morras R., Pöppel W. G. L., 2005, A&A, 440, 775
Kelly B. C., Bechtold J., Siemiginowska A., 2009, ApJ, 698, 895
Laor A., 1991, ApJ, 376, 90
Makishima K., Maejima Y., Mitsuda K., Bradt H. V., Remillard R. A., Tuohy I. R., Hoshi R., Nakagawa M., 1986, ApJ, 308, 635
Misra R., Harikrishnan K. P., Ambika G., Kembhavi A. K., 2006, ApJ, 643, 1114
Mitsuda K. et al., 1984, PASJ, 36, 741
Morrison R., McCammon D., 1983, ApJ, 270, 119
Mushotzky R., Edelson R., 2011, The Astron. Telegram, 3458
Mushotzky R. F., Done C., Pounds K. A., 1993, ARA&A, 31, 717
Noda H., 2016, X-ray Studies of the Central Engine in Active Galactic Nuclei with Suzaku, Springer Theses. Springer Science+Business Media, Singapore
Novikov I. D., Thorne K. S., 1973, in Dewitt C., Dewitt B. S., eds, Black Holes (Les Astres Occlus). Gordon and Breach, London, p. 343
Pal M., Dewangan G. C., Connolly S. D., Misra R., 2016b, MNRAS, preprint (arXiv:1612.01369)
Pal M., Dewangan G. C., Misra R., Pawar P. K., 2016a, MNRAS, 457, 875
Pounds K. A., Reeves J. N., King A. R., Page K. L., O'Brien P. T., Turner M. J. L., 2003, MNRAS, 345, 705
Proust D., 1990, IAU Circ., 5134
Quintana E. V. et al., 2010, SPIE, 7740, 77401X
Rajesh S. R., Mukhopadhyay B., 2010, MNRAS, 402, 961
Ross R. R., Fabian A. C., 2005, MNRAS, 358, 211
Schreiber T., Schmitz A., 1996, Phys. Rev. Lett., 77, 635
Schreiber T., Schmitz A., 1997, Phys. Rev. E, 55, 5443
Schurch N. J., Done C., 2007, MNRAS, 381, 1413
Schurch N. J., Done C., 2008, MNRAS, 386, L1
Schurch N. J., Done C., Proga D., 2009, ApJ, 694, 1
Shakura N. I., Sunyaev R. A., 1973, A&A, 24, 337
Strüder L. et al., 2001, A&A, 365, L18
Theiler J., Eubank S., Longtin A., Galdrikian B., Doyne Farmer J., 1992, Phys. D Nonlinear Phenomena, 58, 77
Titarchuk L., 1994, ApJ, 434, 570
Tripathi S., Misra R., Dewangan G., Rastogi S., 2011, ApJ, 736, L37
Turner M. J. L. et al., 2001, A&A, 365, L27
Volonteri M., Madau P., Quataert E., Rees M. J., 2005, ApJ, 620, 69
Zimmermann H.-U., Boller T., Döbereiner S., Pietsch W., 2001, A&A, 378, 30
Zoghbi A., Fabian A. C., 2011, MNRAS, 418, 2642
Zu Y., Kochanek C. S., Peterson B. M., 2011, ApJ, 735, 80
Zu Y., Kochanek C. S., Kozłowski S., Udalski A., 2013, ApJ, 765, 106

This paper has been typeset from a TEX/LATEX file prepared by the author.